How Microtubules Get Fluorescent Speckles

Clare M. Waterman-Storer and E. D. Salmon
Department of Biology, University of North Carolina, Chapel Hill, North Carolina 27599 USA

ABSTRACT The dynamics of microtubules in living cells can be seen by fluorescence microscopy when fluorescently labeled tubulin is microinjected into cells, mixing with the cellular tubulin pool and incorporating into microtubules. The subsequent fluorescence distribution along microtubules can appear "speckled" in high-resolution images obtained with a cooled CCD camera (Waterman-Storer and Salmon, 1997. *J. Cell Biol.* 139:417–434). In this paper we investigate the origins of these fluorescent speckles. In vivo microtubules exhibited a random pattern of speckles for different microtubules and different regions of an individual microtubule. The speckle pattern changed only after microtubule shortening and regrowth. Microtubules assembled from mixtures of labeled and unlabeled pure tubulin in vitro also exhibited fluorescent speckles, demonstrating that cellular factors or organelles do not contribute to the speckle pattern. Speckle contrast (measured as the standard deviation of fluorescence intensity along the microtubule divided by the mean fluorescence intensity) decreased as the fraction of labeled tubulin increased, and it was not altered by the binding of purified brain microtubule-associated proteins. Computer simulation of microtubule assembly with labeled and unlabeled tubulin showed that the speckle patterns can be explained solely by the stochastic nature of tubulin dimer association with a growing end. Speckle patterns can provide fiduciary marks in the microtubule lattice for motility studies or can be used to determine the fraction of labeled tubulin microinjected into living cells.

INTRODUCTION

Microtubules dynamically assemble in cells from a cytoplasmic pool of α/β tubulin dimers (reviewed by Inoue and Salmon, 1995; Desai and Mitchison, 1998). Each α/β tubulin dimer is 5 nm wide by 8 nm long. Dimers are oriented head to tail at 8-nm spacing along the 13 protofilaments that comprise the 25-nm-diameter cylindrical wall of a microtubule. In 1 μm of microtubule length, there are 125 (1000 nm/8 nm) dimers along each protofilament and 1625 dimers total (125 $\times$ 13 protofilaments). Microtubules grow by dimer association with their ends. Immunofluorescence localization of tubulin has demonstrated the radial distribution of microtubules in cells, with one end, called the minus end, usually oriented toward the centrosome near the cell center, while the other end, the plus end, is generally oriented away from the centrosome and is the primary site of growth. In living cells, microtubule plus ends grow toward the periphery of the cell at 5–7 μm/min velocities, corresponding to association of 135–190 dimers/s. The plus ends often exhibit dynamic instability abruptly switching from growth to shortening at similar or faster velocities for several microns before switching back to growth.

A common method for imaging the assembly dynamics of microtubules in living cells uses time-lapse fluorescence microscopy of microinjected, purified tubulins that have been covalently linked to a fluorophore (Hyman et al., 1991). Labeled tubulin is typically microinjected into tissue cells at a concentration of ~5–10% of the total cellular tubulin pool, which is ~20 μM. Tubulin diffuses rapidly at ~1–2 μm^2/s within the cytoplasm of tissue cells, and the labeled subunits become uniformly distributed in several minutes (Saxton et al., 1984). The fluorescent tubulin subunits become incorporated into microtubules by polymerization reactions, and after 1 h all microtubules in interphase tissue culture cells are fluorescently labeled all along their lengths (Saxton et al., 1984; Shulze and Kirschner, 1986; Waterman-Storer and Salmon, 1997).

Recently we found that labeled microtubules produced in this way in living cells are not uniformly fluorescent, but exhibit "speckled" variations in fluorescence intensity along their lengths (Waterman-Storer and Salmon, 1997). Speckle contrast was particularly noticeable in cells microinjected with very low amounts of labeled tubulin. The fluorescent speckle pattern was detected with a high-resolution digital fluorescence light microscope and a slow-scan cooled charge coupled device (CCD) camera (Waterman-Storer and Salmon, 1997; Salmon et al., 1998). Our instrument has high quantum efficiency and provides images of microtubules with much less noise than the intensified video cameras that were most often used previously to image fluorescent microtubules in living cells. The resolution in the CCD images is close to diffraction limited, with a Rayleigh resolution limit (Inoue and Spring, 1997) of ~0.27 μm for 620 nm X-rhodamine fluorescence. Thus the fluorescent speckle pattern reflects variations in the number of fluorescent tubulin subunits at intervals of ~0.27 μm along the microtubule, and is surprising, given that there are ~440 dimers in this interval.

Our hypothesis is that the normal stochastic association of tubulin dimers with growing microtubule ends generates the fluorescent speckles (Fig. 1). Each time a dimer is added to one of the 13 protofilaments at the growing end, the

Received for publication 12 January 1998 and in final form 13 May 1998.
Address reprint requests to Dr. Clare M. Waterman-Storer, Department of Biology, University of North Carolina, Chapel Hill, NC 27599. Tel.: 919-962-2354; Fax: 919-962-1625; E-mail: waterman@email.unc.edu or tsalmon@email.unc.edu.

0006-3495/98/10/2059/11 $2.00

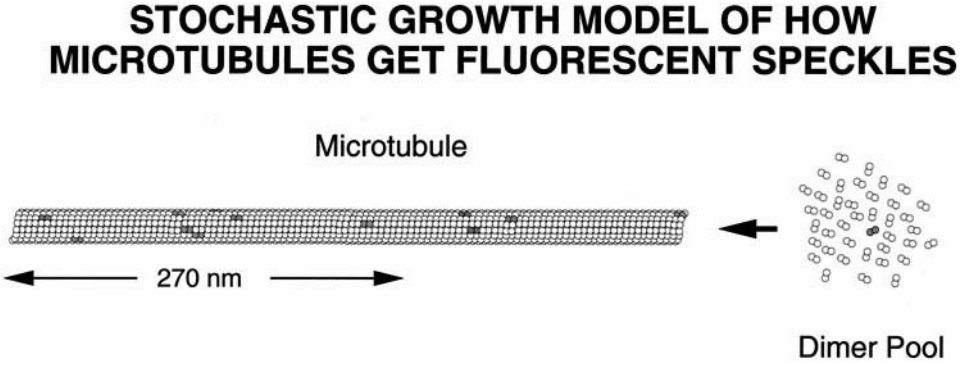

FIGURE 1 A stochastic growth model for the origin of the fluorescent speckle pattern in light micrographs of microtubules grown from a tubulin pool containing a small fraction of labeled dimers. The model assumes that microtubule growth occurs by stochastic tubulin dimer association at protofilament ends in the microtubule cylindrical wall (only seven of the 13 protofilaments are shown).

probability that it will be an X-rhodamine-labeled dimer depends directly on the fraction (f) of labeled dimers in the tubulin pool. If, for example, $f = 2.5\%$, then each time a dimer is added to an end, there is a 1 in 40 chance it will have bound fluorophore. This indicates that over many microns of microtubule growth, the mean number (M) of fluorescent dimers per $N = 440$ dimers in 0.27 μm, the limit of resolution, is $M = Nf = 11$ (2.5% of 440 dimers). The fluorescent speckle pattern is produced by variations from the mean. The standard deviation (SD) from the mean for a stochastic process is given by $SD = (Nf(1 - f))^{0.5}$, which is approximately the square root of the mean for small values of the fraction of labeled tubulin. For a mean value of 11, SD = 3.2. This high standard deviation from the mean for stochastic growth at small fractions of labeled tubulin could explain how microtubules get fluorescent speckles as a result of a high variability in the number of fluorescent tubulin subunits per unit distance along the microtubule. On the other hand, it is also possible that microtubule-associated proteins (MAPs), cellular organelles, dimer oligomers, or some form of cooperative assembly process is necessary to produce the fluorescent speckles seen along microtubules in living cells.

In this paper we test our hypothesis (Fig. 1) on the origins of the microtubule fluorescent speckles by analysis of microtubules assembled in living cells and microtubules assembled from pure tubulins in vitro. In addition, we use computer simulations to demonstrate how the fluorescent speckle pattern in microtubule images can be generated by the product of the stochastic incorporation of labeled dimers into growing ends, the point-spread function of the objective, and the pixel resolution of the camera detector.

MATERIALS AND METHODS

Preparation of porcine brain tubulins

Tubulin was purified from porcine brain by cycles of polymerization and depolymerization, followed by phosphocellulose chromatography as described in Walker et al. (1988). Tubulin was drop frozen in liquid N_2 after passage through a phosphocellulose column and stored at −80°C until use. Porcine brain MAPs were prepared by elution of the phosphocellulose column with 1 M KCl, followed by dialysis against PEM buffer (100 mM piperazine-N,N′-bis(2-ethanesulfonic acid, 2 mM $MgSO_4$, 1 mM EGTA, pH 6.8) containing 1 mM GTP and clarification by centrifugation at 100,000 × g. Just before an experiment, tubulin was thawed, polymerized for 40 min at 37°C in PEM buffer containing 1 mM GTP and 30% glycerol, pelleted by centrifugation at 80,000 rpm in a TLA 100.3 rotor (Beckman Instruments) for 30 min at 37°C, resuspended in PEM buffer, and depolymerized on ice for 30 min. After depolymerization, the tubulin was clarified by centrifugation at 80,000 rpm for 15 min at 4°C in a TLA 100.3 rotor. A small aliquot of the supernatant was removed for determination of protein concentration (using the molar extinction coefficient of 115,000 M/cm^{-1} at 278 nm), while GTP (50 μM or 1 mM) was added immediately to the remaining supernatant.

Tubulin was labeled with X-rhodamine succinimidyl ester (Molecular Probes, Eugene, OR) according to the method of Hyman et al. (1991) and stored frozen at −80°C. The molar dye:protein ratio was determined to be 1.26:1, using the extinction coefficient for X-rhodamine (78,000 M/cm^{-1} at 577 nm). Just before an experiment, the labeled tubulin was thawed, diluted in PEM buffer containing GTP, and clarified as above, and the concentration was determined by measuring the absorbance at 577 nm and using the previously determined dye-to-protein ratio.

Analytical ultracentrifugation

Tubulin (10 μM; either unlabeled or X-rhodamine labeled) in PEM buffer containing 50 μm GTP was subjected to centrifugation at 50,000 rpm at 20°C for 3–4 h in a AN60-Ti rotor in a Beckman Optima XLA analytical ultracentrifuge equipped with absorption optics. A two-sector cell was used; one cell was loaded with 450 μl of buffer, and the other with 350 μl of tubulin solution. For unlabeled tubulin, absorption scans were taken every 2 min at 290 nm, and for X-rhodamine-labeled tubulin, scans were taken similarly at 577 nm. Sedimentation coefficients were determined by the transport method with the XLA Origin software (Beckman) or by nonlinear fitting of the data with the Svedberg shareware (Philo, 1994), using the Fujita function and assuming a single species.

Microinjection of newt lung epithelial cells

Cells on the edge of the epithelial sheet that emanates from an explant of *Taricha granulosa* lung were microinjected with 20 μM X-rhodamine-labeled tubulin in injection buffer (50 mM K-glutamate, 0.5 mM KCl, pH 7.0) as described by Waterman-Storer and Salmon (1997). After recovery from microinjection for 1–2 h, coverslips with adhered microinjected cells were mounted on a slide with the tissue explant between two 70-μm-thick strips of double stick tape spaced ~2 mm apart to form a flow chamber. The chamber was filled with culture medium containing 0.45 units/ml Oxyrase (Oxyrase, Ashland, OH) to retard photobleaching, and the chamber was sealed with valap (1:1:1 vasoline:lanolin:paraffin).

Coassembly of labeled and unlabeled tubulins in vitro

Microtubules were assembled in vitro for 30 min at 37°C in polymerization buffer (PEM buffer containing 1 mM GTP and 4% dimethyl sulfoxide)

from mixtures of various ratios of X-rhodamine-labeled tubulin and unlabeled tubulin at a final total concentration of 20 μM tubulin. In some cases, 0.4 mg/ml MAPs were included in the polymerization mixture. Microtubules were pelleted for 15 min in a microfuge, then resuspended by trituration to the original volume in PEMT buffer (PEM buffer containing 10 μM taxol and 1 mM GTP). Just before imaging, microtubules were diluted 1:20 in PEMT containing 1 mM AMP-PNP and 0.45 units/ml Oxyrase. Microtubules were imaged in flow chambers assembled as described above. To cause microtubules to adhere to the surface of the coverslip, the chamber was filled with a 1:20 dilution (in PEM buffer) of interphase arrested *Xenopus* egg extract (prepared as described by Parsons and Salmon, 1997) and incubated for 10 min in a humid chamber to allow microtubule-based motor proteins in the extract to adhere to the coverslip surface. The chamber was then washed three times with PEM buffer and once with PEMT containing 1 mM AMP-PNP and 45 units/ml Oxyrase. The diluted microtubules were then added to the chamber, incubated for 10 min in a humid chamber, and rinsed once with PEMT containing 45 units/ml Oxyrase and 1 mM AMP-PNP before the chamber was sealed with valap.

Image acquisition

Digital fluorescence images of living cells injected with X-rhodamine-labeled tubulin or microtubules assembled in vitro were acquired with the multimode fluorescence microscope system described by Salmon et al. (1998). This consists of a Nikon Microphot FXA equipped with a 60×/1.4 NA Plan Apo DIC objective, 1.25 body tube magnifier, 1.5× projection magnifier to the camera, and epiillumination provided by a HBO100 mercury arc lamp. Illumination wavelength, intensity, and exposure time were selected by a dual filterwheel apparatus (Metaltek, Raleigh, NC) containing an electronically controlled shutter, a neutral density filterwheel, and an excitation filterwheel with a filter for X-rhodamine (570 nm). Shutter and filterwheel timing and position were controlled by a Ludl (Hawthorne, NY) controller and MetaMorph software (Universal Imaging Corp., Media, PA). Fluorescence images were collected with a Hammamatsu C-4880 cooled CCD camera, which has 12 μm square pixels and a 12-bit linear range of photon detection (see Salmon et al., 1998). For time-lapse imaging of microtubules in living cells, images were acquired at 7-s intervals in 1–2-s exposures, with appropriate neutral density filters in the excitation light path, as described by Waterman-Storer and Salmon (1997).

Data analysis

All position, length, and intensity measurements on digital images were made using the analysis functions of the MetaMorph software (Universal Imaging, West Chester, PA) and analyzed with Microsoft Excel 97 spreadsheet software. A pixel-to-distance conversion factor was determined from an image of a 10-μm stage micrometer. For microtubules assembled in vitro, sets of "data images" of microtubules bound to coverslips coated with *Xenopus* extracts were acquired for each fraction of labeled tubulin examined. Exposure times were adjusted and illumination was attenuated with neutral density filters appropriately, so that the microtubule brightness was about half the camera saturation (~2000 of 4096 gray levels). For each set of data images, a corresponding series of 10 slightly defocused background images of a coverslip surface coated with *Xenopus* extract, but no microtubules, was acquired at the same settings. The background images were averaged and subtracted from each of the data images before analysis. For microtubules in living cells, unpolymerized X-rhodamine-labeled tubulin in the cell contributed to the intensity measurement along microtubules. To correct for this, five images from a time-lapse series (the third image in the series being data image) were averaged, and background line scans were taken at three to five pixels to the left and right of the microtubule analyzed, respectively. Intensity values along the two background line scans were averaged, and this "intracellular background" was subtracted from the values of intensity along the microtubule. After background corrections, fluorescence intensity along microtubules was measured using the "line scan" function of MetaMorph, and the values were exported to Excel. Care was taken to center the chosen line at the peak intensity along the 2–4-pixel width of the microtubule image, and no microtubules less than 5 μm long were analyzed. Fluorescence intensity values were then standardized to be equivalent to images taken in 1-s exposures and no neutral density filters. Standardized fluorescence intensity values were obtained by dividing the intensity values by the exposure time and multiplying by $\log^{-1}(\mathrm{OD})$. Mean standardized fluorescence intensity, standard deviation of standardized fluorescence intensity, and contrast (standard deviation/mean) were determined for individual microtubules, and these values were averaged for microtubules within a single cell or assembled from a given fraction of labeled tubulin.

Power spectral analysis of fluorescent speckle patterns along microtubules were obtained with Mathematica software (Wolfram, 1988):

$$\mathrm{Powerspec} = |\mathrm{FT}(\mathrm{datanorm} - 1)|^2 \qquad (1)$$

where *FT* is the Fourier transform function, and datanorm is the standardized fluorescence intensity values along a microtubule divided by the mean. For in vivo, in vitro, and computer-simulated microtubules, fluorescence intensity distributions for individual microtubules 5–16 μm in length were ligated together to obtain a composite fluorescence distribution between 80 and 100 μm in length for power spectral analysis.

RESULTS

Microtubule fluorescent speckle distributions in vivo

Individual microtubules in the lamella of a living newt lung epithelial cell that had previously been microinjected with low levels of X-rhodamine-labeled tubulin clearly show speckled variations in fluorescence along their lengths (Fig. 2 *A*). The pattern of fluorescent speckles appeared random by several criteria. The pattern was different in different regions along a microtubule (Fig. 2 *A*) and between different microtubules (Figs. 2 *A* and 3). We calculated a power spectrum on the values of standardized fluorescence intensity for 14 microtubules in five cells, ligated together for 100.08 μm of total polymer. This analysis revealed that there were many peaks of spatial frequency in the fluorescence intensity distribution, but no dominant periodicity in the fluorescent speckle pattern (Fig. 4 *A*).

We also found that the speckle pattern did not vary over time (compare portions of the *graphs to the left of the arrows* in Fig. 5), unless shortening and regrowth of the microtubule occurred (compare the portions of *graphs to the right of the arrows* in Fig. 5). This indicates that the speckle pattern is intrinsic to the microtubule lattice and changes only with disassembly and reassembly at a microtubule end.

We measured "speckle contrast" by calculating the standard deviations of the variations in standardized fluorescence intensity in the line scans along the length of microtubules (Fig. 3) and dividing this value by their mean standardized fluorescence intensity. The average speckle contrast from five microtubules in one cell was 0.256 (range = 0.200–0.421, n = 5 microtubules, total polymer = 29.52 μm), whereas in another cell it was 0.317

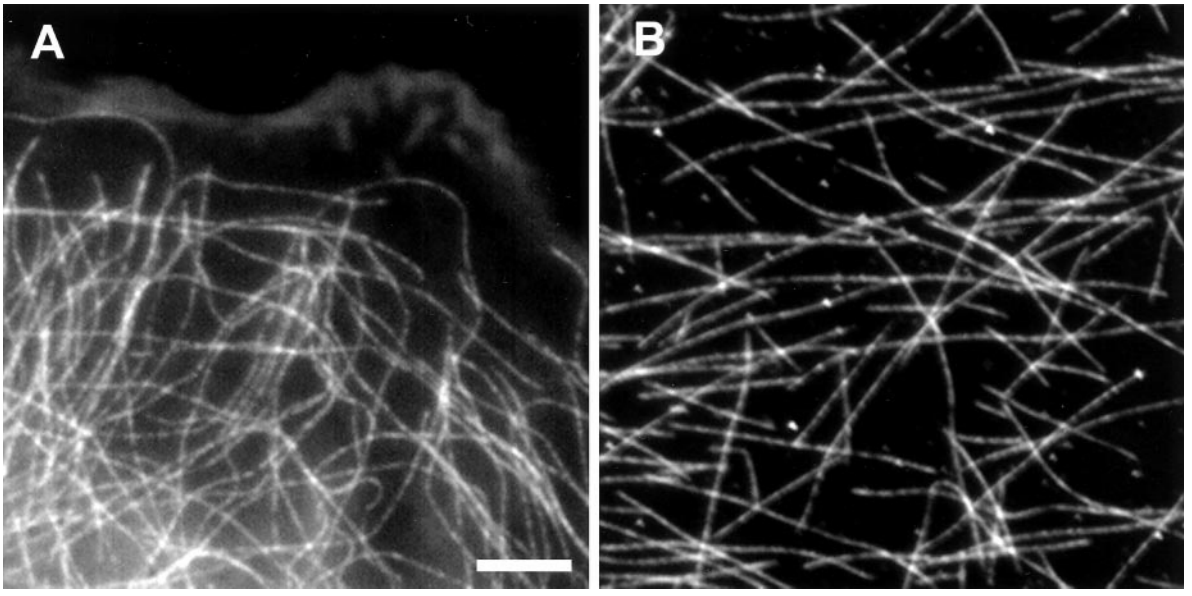

FIGURE 2 A comparison of the random speckle pattern of fluorescence along microtubules for (*A*) a living cell microinjected with X-rhodamine-labeled tubulin, and for (*B*) microtubules assembled in vitro from 5% X-rhodamine-labeled tubulin, 95% unlabeled tubulin. Scale = 5 μm.

(range = 0.263–0.362, n = 5 microtubules, total polymer = 32.87 μm) (Table 1).

Microtubule fluorescent speckle distribution in vitro

To test whether cellular factors such as MAPs or organelles contribute to the fluorescent speckle distribution and to determine how mean contrast depends on the fraction of labeled dimers, we examined fluorescence distribution along microtubules assembled in vitro from mixtures of pure tubulin consisting of various fractions of X-rhodamine-labeled and -unlabeled dimers. Microtubules assembled from pure tubulin containing from 1.25% to 50% labeled dimers exhibited speckled patterns of varying fluorescence intensity along their length (Figs. 2 *B* and 6). The speckle

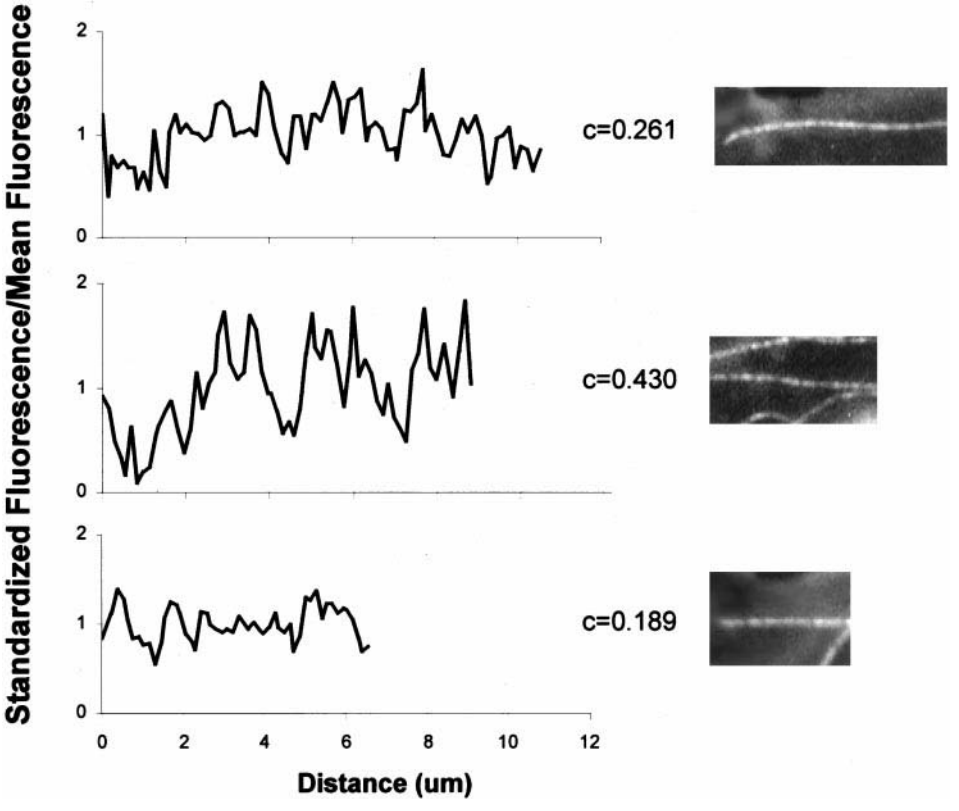

FIGURE 3 Quantitation of the speckle pattern by fluorescence intensity line scans (*left*) along images of microtubules (*right*) obtained from three different living cells. Standardized fluorescence values in the plots on the left are from fluorescent line scans corrected for background fluorescence contributions as described in Materials and Methods. c is the contrast of the fluorescent speckles obtained by the standard deviation of the standardized fluorescence values from the mean divided by the mean fluorescence along a microtubule. Note that no two microtubules exhibit the same fluorescent speckle pattern.

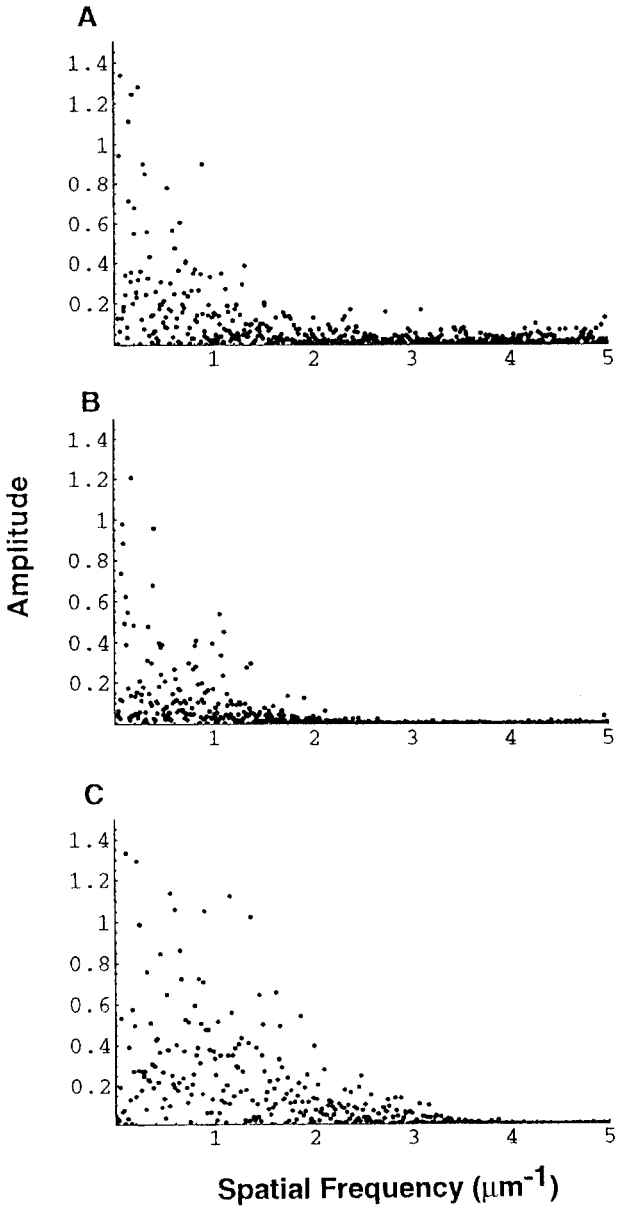

FIGURE 4 Comparison of the power spectra of fluorescent speckles for microtubules (*A*) in living cells microinjected with labeled tubulin; (*B*) assembled in vitro from 1.25% labeled tubulin; and (*C*) computer simulated with 1.25% labeled tubulin, and a camera resolution of 112 nm.

patterns for microtubules assembled in vitro appeared to be random, like the microtubules in living cells (Fig. 3). This was confirmed by the broad spectral distribution of power spectra of standardized fluorescence intensities for ~100 μm of ligated lengths of microtubule polymer for each fraction of labeled tubulin examined in vitro. For example, the power spectrum for $f = 1.25\%$ is shown in Fig. 4 *B*. This shows a pattern similar to that of the power spectrum obtained for microtubules in vivo (Fig. 4 *A*). The standard deviations of the fluctuations in standardized fluorescence relative to the mean standardized fluorescence depended on the fraction of labeled tubulin, and speckle contrast increased progressively with lower fractions of labeled tubulin (Figs. 6 and 7). Addition of purified brain MAPS at 0.4 mg/ml, a concentration that strongly promotes and stabilizes microtubule assembly, had no noticeable effect on speckle contrast over the fraction range tested (Fig. 7 and Table 1). Thus neither MAPs nor other cellular factors are required for generation of speckle patterns, and speckle contrast depends mainly on the fraction of labeled tubulin.

One possible explanation for the fluorescent speckle pattern is that the presence of a hydrophobic fluorophore on tubulin causes the X-rhodamine-labeled tubulin to self-associate and incorporate into microtubules as brightly labeled oligomers. To test this possibility, we determined the size distribution of our X-rhodamine-labeled tubulin by analytical ultracentrifugation at the concentration (10 μM) used to assemble speckled microtubules in vitro. Both 100% labeled tubulin ($n = 3$) and unlabeled tubulin ($n = 3$) sedimented as single monotonic 5.6S peaks (data not shown). Therefore, the polymerizing fluorescent subunit in pure tubulin mixtures is the tubulin dimer as diagrammed in Fig. 1, and not oligomers of fluorescent dimers.

Computer simulation of fluorescent microtubule images based on the stochastic growth model

We used computer simulations in Mathamatica software (Wolfram, 1988) to test how the fluorescent speckle pattern in microtubule images is generated by the product of 1) the stochastic incorporation of labeled tubulin into growing ends; 2) the point-spread function of the objective; and 3) the pixel resolution of the camera detector. The example described here is for a fraction of labeled tubulin of $f = 2.5\%$. There are three parts to the simulation.

First, Monte Carlo simulations were used to calculate the number of fluorescently labeled subunits at 8-nm intervals along a microtubule grown to a length of 16.384 μm. The assumptions in this simulation are 1) the tubulin dimer pool is homogeneous, except that a fraction has fluorescent label; 2) there is one fluorophore per dimer; 3) tubulin association at the growing end is random (Fig. 1); and 4) the unit distance along the microtubule is the length of the dimer, 8 nm. In the simulation, when a dimer is added to the growing end (Fig. 1), a random number is obtained between 0 and 1. If the random number is less than the fraction of labeled tubulins (e.g., $f = 2.5\%$), then the dimer is labeled with a 1, otherwise it is 0. For each 8-nm increment of growth, 13 dimers are added and their fluorescent values are summed, because there are 13 protofilaments in the microtubule wall:

$$\mathrm{MT}(j) = \mathrm{Table}[(\mathrm{Sum}(\mathrm{If}\,\mathrm{Random}[\,], f, 1, 0), \{i, 1,13\}), \{j, 1,2048\}] \quad (2)$$

Fig. 8 *A* plots the number of fluorophores per 8-nm interval along a fluorescent microtubule simulated by Eq. 2 and using $f = 2.5\%$. For this simulation the average number of fluorophores per 8-nm interval is 0.325, the number expected from the product of $13f$.

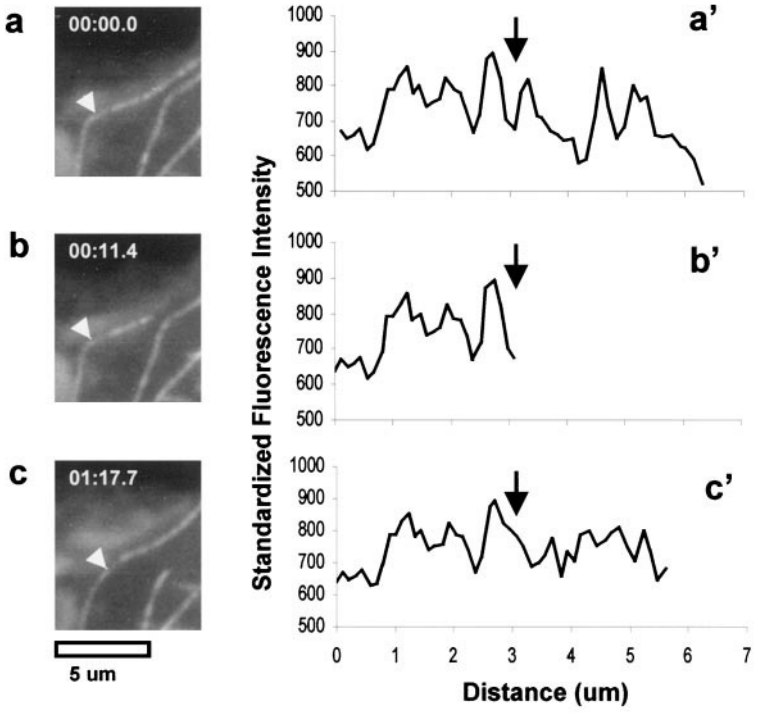

FIGURE 5 Sequential line scans along individual microtubules show that the random pattern of fluorescent speckles is produced during microtubule growth. On the left are sequential images, *a*, *b*, *c*, of the same microtubule from a time-lapse recording. Time is given in minutes: seconds on each frame. The corresponding line scan plots of standardized fluorescence intensity *a′*, *b′*, and *c′* are on the left. The arrowheads in *a*, *b*, and *c* indicate the starting point (position 0 μm) for the line scans in *a′*, *b′*, and *c′*. Between *a* and *b*, the microtubule begins shortening from its upper end. When frame *b* was taken, the microtubule was still shortening. By the time frame *c* was taken, the microtubule end stopped shortening and regrew beyond the field of view at the upper right. The history of microtubule shortening and regrowth can be seen by comparing the line scans on the right. The arrows (*right*) mark the position along the microtubule where regrowth occurred (see text). Note that in *c′* the fluorescent speckle pattern after regrowth is completely different from the pattern before shortening.

Second, the simulated fluorescent microtubule obtained from Eq. 2 was convolved with the theoretical point-spread function of our microscope objective lens to generate the ideal image projected by the objective onto our cooled CCD detector. Because of the finite numerical aperture (NA) of the objective, a point source of light in the specimen is spread into an Airy disk interference pattern in the image (Born and Wolf, 1965). The radius, *r*, of this Airy disk for a fluorescent point source of light is given by $r = 0.61\ \lambda/\mathrm{NA}$, where λ is the wavelength of light. For $\lambda = 620$ nm, NA = 1.4, then $r = 0.27\ \mu$m. Thus the image of each 8-nm fluorescent dimer is spread out by this objective point-spread function into 0.54-μm-diameter spots in the image. The square of the amplitude of the objective point spread function (PSF) is plotted in Fig. 8 *B* from calculations in our Mathematica simulations by

$$\mathrm{PSF} = \mathrm{Table}[(2\mathrm{Bessel}[1,34(j - 1024 + 0.0001)]/ 34(j - 1024 + 0.0001))^2, \{j, 1,2048\}] \quad (3)$$

where 34 is the scale factor needed to make the first minima of the Bessel function correspond to the Airy disk first minima at $r = 0.27\ \mu$m, which is equal to 34 increments of 8 nm along the microtubule. The image (MTobjn) produced by the objective (Fig. 8 *C*) was obtained by convolving the PSF with the simulated microtubule:

$$\mathrm{MTobj} = \mathrm{Chop}[\mathrm{InverseFourier}[2048^{0.5}\mathrm{MT}]\mathrm{Fourier}[\mathrm{PSF}]] \quad (4)$$

and normalizing the result by

$$\mathrm{MTobjn} = \mathrm{MTobj} * \mathrm{Mean}[\mathrm{MT}]/\mathrm{Mean}[\mathrm{MTobj}] \quad (5)$$

The normalization in Eq. 5 makes the total fluorescence in the objective image the same as in the original simulated microtubule.

Finally, the resolution in the objective image is further reduced by the finite size of the picture element (pixel) detectors in our CCD camera, which are 12 μm square. We project the objective image onto this detector with a magnification of 112.5× (60× objective, 1.25× magnification in the body tube and 1.5× in the magnifier to the camera). At this magnification, a pixel width of 12 μm corresponds to ~112 nm, or 14 increments of 8 nm along the microtubule. There are 146 intervals of 112 nm in a 16.384-μm-long microtubule. The camera image of the microtubule (MTcam) is plotted in Fig. 8 (*bottom trace*) from the following:

$$\mathrm{MTcam} = \mathrm{Table}[(\mathrm{Sum}[\mathrm{MTobjn}[i]], \{i, 14j - 13, 14j\}), \{j, 1, 146\}] \quad (6)$$

As can be seen in Fig. 8 (*bottom trace*), the random fluorescent fluctuations along the simulated microtubule are typical of the fluorescence speckles of the image of microtubules in the live cells (Figs. 2 *A*, 3, and 4). To see how speckle contrast changes with the fraction of labeled tubulin in the simulated microtubules, we simulated microtubules (Eqs. 2–6) for fractions of labeled tubulin corresponding to the in vitro studies, $f = 1.25\%$, 2.5%, 5%, 10%, 25%, and 50%. Fig. 9 shows that speckle contrast increases in the simulated microtubules as the fraction of labeled tubulin decreases—a result typical of the in vitro assembled microtubules (Fig. 6).

TABLE 1 Analysis of microtubule speckle contrast for microtubules assembled from various fractions of X-rhodamine-labeled and unlabeled pure tubulin in vitro and microtubules in living cells microinjected with labeled tubulin

Fraction X-rhodamine tubulin	*n* (MTs)	Total polymer (μm)	Mean standardized fluorescence	Mean standard deviation	Mean contrast (SD/mean)
50%	10	89.43	19947.86	1258.397	0.063
50% + MAPs*	10	71.80	19278.69	1366.40	0.071
50% Simulated**					0.05
25%	10	116.66	8171.79	712.26	0.087
25% + MAPs	10	101.82	11313.07	1001.47	0.088
25% Simulated					0.08
10%	10	96.44	4774.67	493.63	0.105
10% + MAPs	10	98.70	5049.21	545.20	0.110
10% Simulated					0.14
5%	10	104.57	1754.29	235.77	0.134
5% + MAPs	10	102.75	2549.19	372.66	0.147
5% Simulated					0.19
2.5%	10	88.84	639.06	123.28	0.190
2.5% + MAPs	12	78.06	1213.79	218.39	0.199
2.5% Simulated					0.28
1.25%	10	109.99	442.58	104.58	0.232
1.25% + MAPs	10	86.09	592.17	142.99	0.241
1.25% Simulated					0.42
Living cell 1	5	29.52	778.82	199.28	0.256
Living cell 2	5	32.87	1241.64	394.00	0.317

*Microtubules assembled in the presence of 0.4 mg/ml porcine brain MAPs.
**Theoretical contrast determined from computer simulations of microtubule assembly.

To quantitatively compare the simulation results with the in vitro microtubule data, average values of contrast were obtained from five simulations at each value of f; these contrast values are plotted in Fig. 7 for comparison to the values measured for the microtubules assembled in vitro. This shows that speckle contrast for both the measured data and that for the simulated data have the same general dependency on the fraction of labeled tubulin and have similar values at higher fractions of labeled tubulin. However, in comparison to the measured data, the contrast values for the simulated data become significantly higher at lower fractions of labeled tubulin. We also obtained power spectra for simulated camera images of microtubules. In Fig. 4 *C*, the example obtained for $f = 1.25\%$ is shown; this is very similar to the power spectra obtained from the analysis of images of microtubules assembled in vitro from 1.25% labeled tubulin (Fig. 4 *B*) and for microtubules in living cells microinjected with labeled tubulin (Fig. 4 *A*).

The accuracy of the computer simulations was tested by comparing the average contrast values determined by the Monte Carlo simulations to values of contrast calculated by statistical expectations of random dimer addition to a growing end. The general formula for the speckle contrast between adjacent regions along a microtubule is

$$\text{Contrast} = \text{SD/Mean} = (Nf(1-f))^{0.5}/Nf \qquad (7)$$

where N is the number of dimers in a region, and f is the fraction of labeled tubulin in the tubulin pool. For $N = 440$ dimers, Eq. 7 gives values nearly identical to those from the above computer simulations over the fractions of labeled tubulin tested (Fig. 7). Therefore, the computer simulations accurately represent the fluorescence speckle patterns predicted by the random chance aspects of tubulin association with growing ends.

DISCUSSION

Our model for microtubule assembly and the generation of fluorescent speckles (Fig. 1) is based on the assumption of stochastic association of tubulin dimers with growing microtubule ends. It predicts well the fluorescent speckles of both microtubules assembled in vitro from pure tubulin and those assembled in cells. This provides evidence that in living cells the fundamental mechanism of microtubule assembly is due solely to the addition of tubulin dimers from microtubule ends; subunit exchange along the lattice of microtubules and assembly by addition of tubulin oligomers are unlikely. Cellular organelles, dimer oligomers, MAPs, or other cellular factors are not required to generate fluorescent speckles.

As predicted by the computer simulations and statistical analysis, the mean speckle contrast of microtubules assembled in vitro from pure tubulin increases substantially as the fraction of labeled tubulin decreases below 10%, and particularly below 5%. Why the measured speckle contrast at

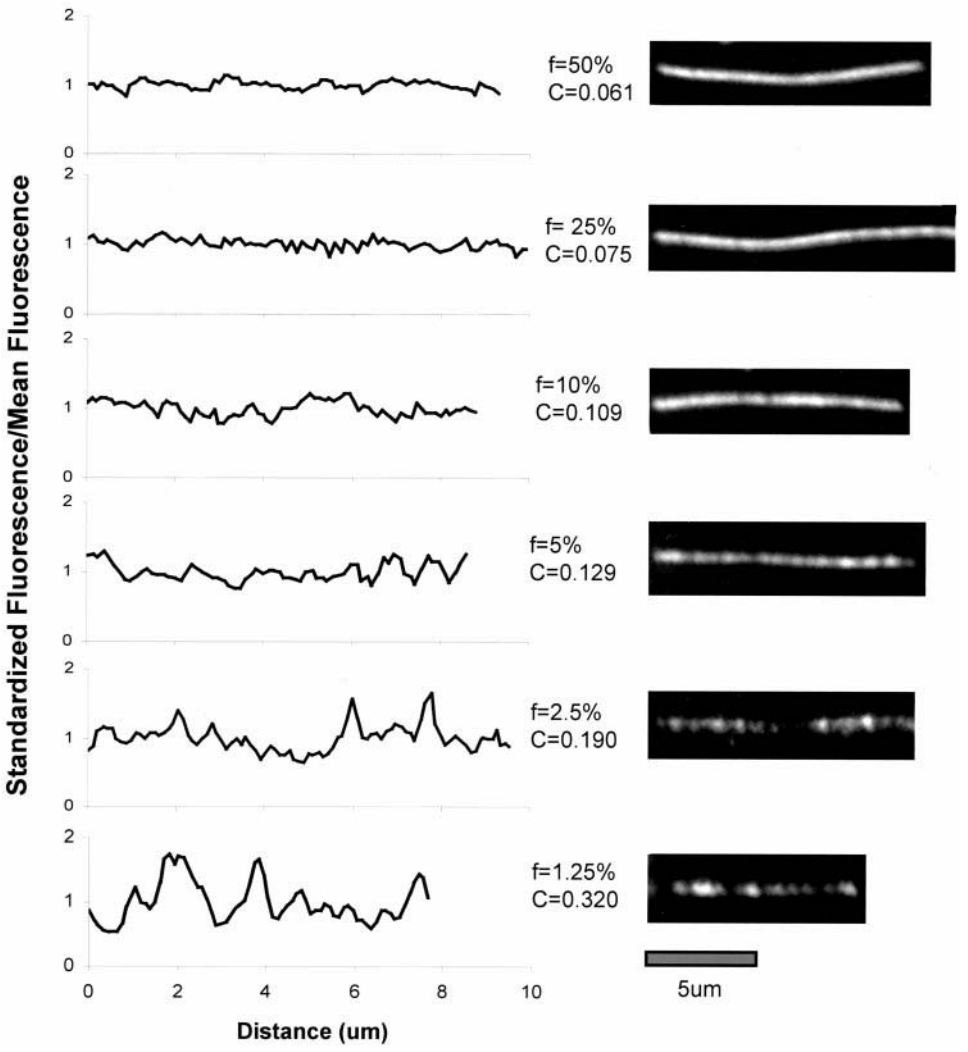

FIGURE 6 The amplitude of the fluorescent speckle pattern along microtubules assembled in vitro depends on the fraction of labeled tubulin dimers. On the left are the line scans of the example microtubules shown on the right for fractions, *f*, of labeled tubulin ranging from 50% (*top*) to 1.25% (*bottom*). See legend for Fig. 3 for details about the line scans and contrast values, *c*. Note that speckle contrast increases substantially for lower fractions of labeled dimer.

low fractions of labeled dimers is not as high as predicted by theory is unknown. A likely explanation is that speckle contrast is reduced at low values of labeled tubulin by background "noise" from variations in the coverslip preparation, autofluorescence in the specimen and the optical system, and noise in the camera. This background noise is a more significant factor as the fraction of labeled tubulin decreases, because the fluorescence intensity of the microtubule also decreases. At higher fractions of labeled tubulin, microtubule fluorescence brightens, and the background noise is no longer a significant factor. For example, the mean (M) number of fluorescent dimers expected in a resolvable region of 0.27 μm or 440 dimers is $M = Nf =$ 5.5, 11, 22, 44, 110, and 220 for $f =$ 1.25%, 2.5%, 5%, 10%, 25%, and 50%. A noise level equivalent to 5.5 fluorophores would significantly reduce the speckle contrast for $f =$ 1.25%, but have relatively little effect for fractions of 10% or more, because the mean number of fluorophores is substantially greater.

The above considerations also indicate why the speckles were not obvious in previous studies in which microtubules were assembled with fluorescently labeled dimers. The cooled CCD camera used in our studies has a high quantum efficiency (65% at 620-nm wavelength) and very low noise (less than 10 electrons; Salmon et al. 1998). As a consequence, high-quality images of microtubules could be obtained at low fractions of labeled tubulin where speckle contrast is greatest. Higher concentrations of fluorescent tubulin are required to obtain images of microtubules with cameras or optical systems that have poorer sensitivity and higher noise. For fractions above 5%, speckle contrast would be reduced (Fig. 6) and perhaps would not be obvious, because of camera noise typical of the intensified video cameras often used previously to image individual fluorescent microtubules in living cells (see, for example, Shelden and Wadsworth, 1993).

One application of the fluorescent microtubule speckles is in the measurement of the fraction of labeled tubulin in microinjected cells. The speckle contrast data in Fig. 7 and Table 1 for the in vitro assembled microtubule provide a calibration curve for our imaging system. For example, the mean speckle contrast measured for microtubules in the microinjected living cells, 0.26–0.32, is somewhat larger than the contrast measured for the smallest fraction of

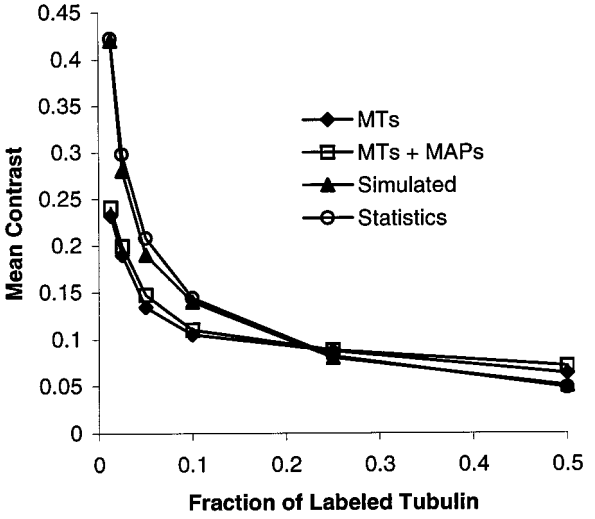

FIGURE 7 Mean speckle contrast for microtubules assembled in vitro and simulated depends on the fraction of labeled tubulin. Microtubules were assembled in vitro from pure tubulin or pure tubulin in the presence of 0.4 mg/ml porcine brain MAPs as a function of the fraction of labeled tubulin dimers. Each in vitro data point represents the average contrast of 10 microtubules. The simulated microtubule values represent the average from five microtubules for each fraction of labeled tubulin. See text for details about the simulated microtubules and the statistical expectations.

labeled tubulin for microtubules assembled in vitro, 0.235 at $f = 1.25\%$. This comparison indicates that the fraction of labeled tubulin in the microinjected cells we analyzed is likely to be ~1% of the total cytoplasmic tubulin pool. It should be noted that the fluorescent speckles seen in our images of living cells microinjected with labeled tubulin are not to be confused with discontinuous and punctate immunofluorescent labeling of microtubules in fixed cells by anti-tubulin antibodies and fluorescent secondary antibodies (see, for example, figure 1 *B* in Waterman-Storer et al., 1995). The discontinuities of microtubule labeling in immunofluorescence images are generally caused by improper dilution of antibodies or fragmentation of the microtubules due to improper fixation conditions.

Another important application of our ability to image fluorescent speckles along microtubules is that they provide fiduciary marks in the microtubule lattice. By virtue of the marks in the microtubule lattice, changes in microtubule length can be assigned unambiguously to assembly/disassembly reactions at either end. In addition, the speckles can be used to detect and measure microtubule translocation through the cytoplasm, during which the microtubule ends can be either growing or shortening. We have been able to use this method to show that cytoplasmic microtubules exhibit both "treadmilling," in which net assembly occurs at the plus end and net disassembly occurs at the minus end, as well as occasional brief translocations through the cytoplasm (Waterman-Storer, 1997).

The ability to image and analyze speckle patterns in fluorescence in living cells should also prove useful in other applications, such as analysis of microtubule poleward flux

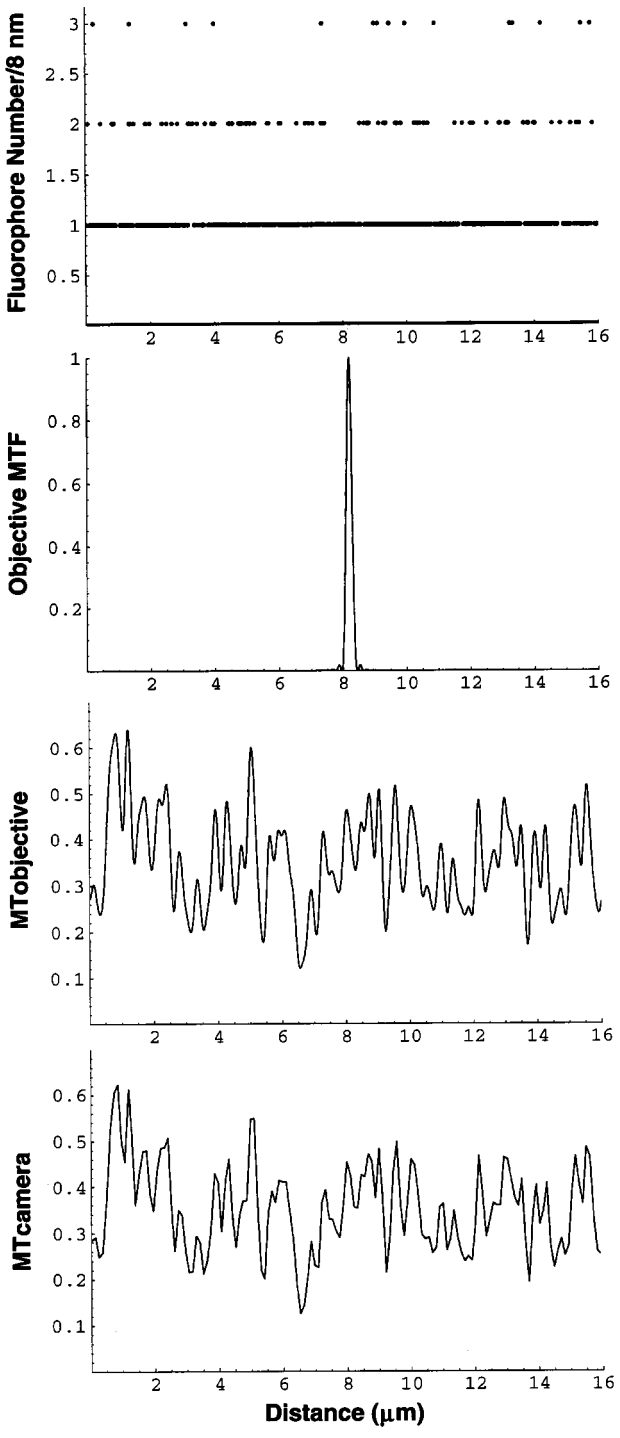

FIGURE 8 Computer simulation of microtubule growth from a tubulin pool containing a 2.5% fraction of fluorescently labeled dimers. (*A*) The number of fluorescent dimers along a simulated microtubule at 8-nm increments as obtained from Eq. 2. (*B*) The objective point spread function (PSF) obtained from Eq. 3. (*C*) The objective image of the simulated microtubule (MTobjective) obtained by convolving the fluorescent distribution in *A* with the objective PSF, as given by Eqs. 4 and 5. (*D*) The camera image of the microtubule (MTcamera) after modification of Mtobjective by the pixel resolution of the camera used in our studies (Eq. 6). See text for details.

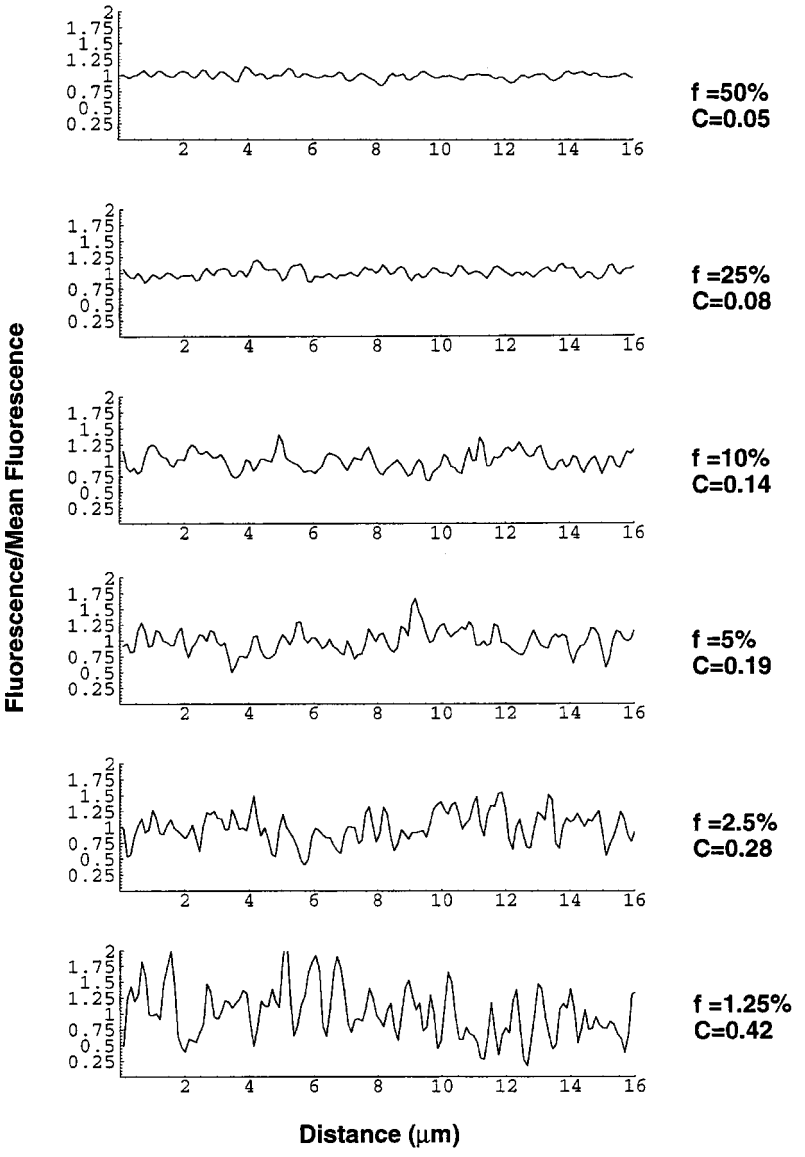

FIGURE 9 The camera image of normalized fluorescence distributions along computer-simulated microtubules (*left*) for various fractions (*f*) of labeled tubulin (*right*). The camera image plots, MTcamera, were obtained from Eqs. 2–6 and normalized by the mean fluorescence of the simulated microtubule image. *c* is the mean speckle contrast averaged for five simulated microtubules at each fraction of labeled tubulin. See text for details.

in mitotic spindles (Mitchison and Salmon, 1992), the movement of microtubules released from the centrosome (Keating et al., 1997), the turnover of fluorescently labeled MAPs, and actin and intermediate filament dynamics. However, our analysis indicates that high speckle contrast is achieved only for very low fractions of labeled protein. As a result, application of the fluorescent speckle method requires a microscope and camera system that can detect at 0.27-μm resolution fluorescence from a few fluorophores with great clarity. In this regard, Kinosita and co-workers (Sase et al., 1995) have been able to measure the motility of single fluorophores on actin filaments in vitro using a conventional epifluorescence microscope. These methods provide simple means for observing molecular dynamics in a variety of applications.

This paper is dedicated to Fred Fay, who pioneered the development of the high-resolution digital image acquisition instrumentation used in our study, in addition to his efforts to improve deconvolution methods and obtain "superresolution" in fluorescence light microscopy (Fay, 1995; Carrington et al., 1995).

We thank Christian R. Lombardo of the University of North Carolina Macromolecular Interactions Facility for his expert assistance in the sedimentation analysis of labeled and unlabeled tubulins.

This work was supported by the National Institutes of Health (GM 24364).

REFERENCES

Carrington, W. A., R. M. Lynch, E. D. Moore, G. Isenberg, K. E. Fogarty, and F. S. Fay. 1995. Superresolution three-dimensional images of fluorescence in cells with minimal light exposure. *Science.* 268:1483–1487.

Desai, A., and T. J. Mitchison. 1997. Microtubule polymerization dynamics. *Annu. Rev. Cell Dev. Biol.* 13:83–117.

Fay, F. S. 1995. Calcium sparks in vascular smooth muscle: relaxation regulators. *Science.* 270:588–589.

Hyman, A., D. Drechsel, D. Kellogg, S. Salser, K. Sawin, P. Steffen, L. Wordeman, and T. Mitchison. 1991. Preparation of modified tubulins. *Methods Enzymol.* 196:478–485.

Inoue, S., and E. D. Salmon. 1995. Force generation by microtubule assembly/disassembly in mitosis and related movements. *Mol. Biol. Cell.* 6:1619–1640.

Inoue, S., and K. Spring. 1997. Video Microscopy, 2nd Ed. Plenum, New York.

Keating, T. J., J. G. Peloquin, V. I. Rodionov, D. Momcilovic, and G. G. Borisy. 1997. Microtubule release from the centrosome. *Proc. Natl. Acad. Sci. USA.* 94:5078–5083.

Mitchison, T. J., and E. D. Salmon. 1992. Poleward kinetochore fiber movement occurs during both metaphase and anaphase-A in newt lung cell mitosis. *J. Cell Biol.* 119:569–582.

Parsons, S. F., and E. D. Salmon. 1997. Microtubule assembly in clarified *Xenopus* egg extracts. *Cell Motil. Cytoskeleton.* 36:1–11.

Philo, J. S. 1994. *In* Modern Analytical Ultracentrifugation: Acquisition and Interpretation of Data for Biological and Synthetic Polymer Systems. T. M. Shuster and T. M. Laue, editors. Birkhäuser, Boston. 156–170.

Salmon, E. D., S. L. Shaw, J. Waters, C. M. Waterman-Storer, P. S. Maddox, E. Yeh, and K. Bloom. 1998. A high resolution multimode microscope system. *Methods Cell. Biol.* 56:185–214.

Sase, I., H. Miyata, J. E. T. Corrie, J. S. Craik, and K. Kinosita, Jr. 1995. Real-time imaging of single fluorophores on moving actin with an epifluorescence microscope. *Biophys. J.* 69:323–328.

Saxton, W. M., D. L. Stemple, R. J. Leslie, E. D. Salmon, M. Zavortink, and J. R. McIntosh. 1984. Tubulin dynamics in cultured mammalian cells. *J. Cell Biol.* 99:2175–2186.

Shelden, E., and P. Wadsworth. 1993. Observation and quantification of individual microtubule behavior in vivo: microtubule dynamics are cell-type specific. *J. Cell Biol.* 120:935–945.

Shulze, E., and M. W. Kirschner. 1986. Microtubule dynamics in interphase cells. *J. Cell. Biol.* 102:1020–1031.

Walker, R. A., E. T. O'Brien, N. K. Pryer, M. F. Soboeiro, W. A. Voter, H. P. Erickson, and E. D. Salmon. 1988. Dynamic instability of individual microtubules analyzed by video light microscopy: rate constants and transition frequencies. *J. Cell Biol.* 107:1437–1448.

Waterman-Storer, C. M., S. Karki, and E. L. F. Holzbaur. 1995. The $p150^{Glued}$ component of the dynactin complex binds to both microtubules and the novel actin, centractin. *Proc. Natl. Acad. Sci. USA.* 92:1634–1638.

Waterman-Storer, C. M., and E. D. Salmon. 1997. Actomyosin-based retrograde flow of microtubules in the lamella of migrating epithelial cells influences microtubule dynamic instability and turnover and is associated with microtubule breakage and treadmilling. *J. Cell Biol.* 139:417–434.

Wolfram, S. 1988. Mathematica: A System for Doing Mathematics by Computer. Addison-Wesley, Redwood City, CA.